THE UNIVERSITY OF RHODE ISLAND

University of Rhode Island DigitalCommons@URI

Graduate School of Oceanography Faculty Publications

Graduate School of Oceanography

2013

Geodynamic Evolution of a Forearc Rift in the Southernmost Mariana Arc

Julia M. Ribeiro

Robert J. Stern

See next page for additional authors

Follow this and additional works at: https://digitalcommons.uri.edu/gsofacpubs

The University of Rhode Island Faculty have made this article openly available. Please let us know how Open Access to this research benefits you.

This is a pre-publication author manuscript of the final, published article.

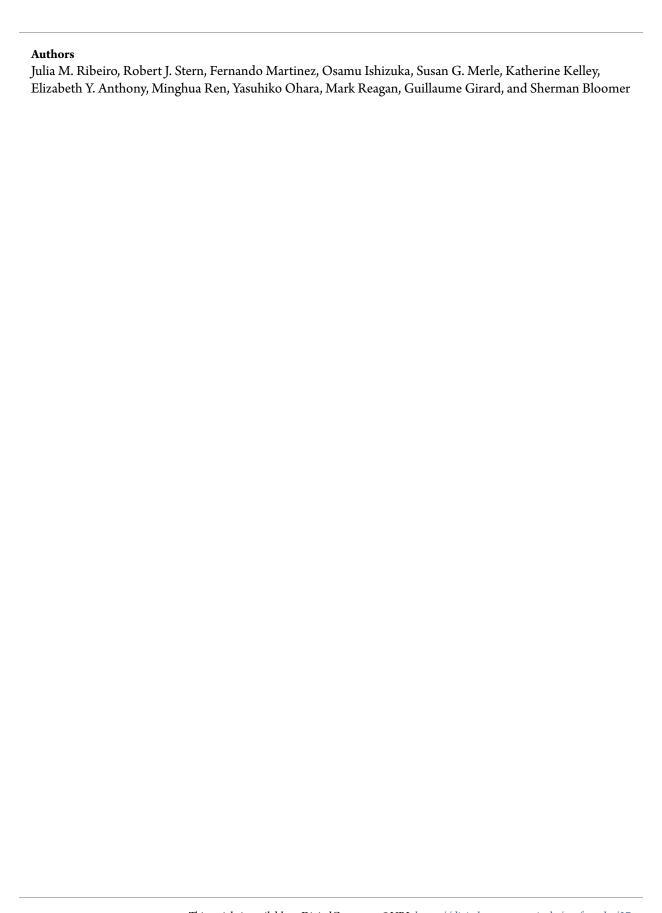
Terms of Use

This article is made available under the terms and conditions applicable towards Open Access Policy Articles, as set forth in our Terms of Use.

Citation/Publisher Attribution

Ribeiro, Julia M., et al. "Geodynamic Evolution of a Forearc Rift in the Southernmost Mariana Arc." *Island Arc* 22.4 (2013): 453-476. Available at: http://dx.doi.org/10.1111/iar.12039

This Article is brought to you for free and open access by the Graduate School of Oceanography at DigitalCommons@URI. It has been accepted for inclusion in Graduate School of Oceanography Faculty Publications by an authorized administrator of DigitalCommons@URI. For more information, please contact digitalcommons@etal.uri.edu.



Geodynamic evolution of a forearc rift in the southernmost Mariana Arc 1

3

2

- Julia M. Ribeiro¹, Robert J. Stern¹, Fernando Martinez², Osamu Ishizuka^{3, 10}, Susan G.
- Merle⁴, Katherine Kelley⁵, Elizabeth Y. Anthony⁶, Minghua Ren⁶, Yasuhiko Ohara^{7, 10}, 4

- 5
- Mark Reagan⁸, Guillaume Girard⁸, Sherman Bloomer⁹
- ¹ Geosciences Department, University of Texas at Dallas, 800 W. Campbell Rd. Richardson, TX 7
- 8 75083-0688, USA
- ² Hawai'i Institute of Geophysics and Planetology, SOEST, University of Hawai'i at Manoa, 680 9
- 10 East-West Rd, POST 602, Honolulu, HI 96822 USA
- ³ Geological Survey of Japan, AIST, Central 7, 1-1-1 Higashi, Tsukuba, Ibaraki 305-8567, Japan 11
- ⁴ Oregon State University, NOAA Vents Program, 2115 SE Oregon State University Dr., 12
- 13 Newport, OR 97365, USA
- ⁵ Graduate School of Oceanography, University of Rhode Island, Narragansett Bay Campus, 14
- 15 Narragansett, RI 02882, USA
- ⁶ University of Texas at El Paso, Department of Geological Sciences, 500 West University 16
- 17 Avenue, El Paso, TX 79968, USA
- ⁷ Hydrographic and Oceanographic Department of Japan, 2-5-18 Aomi, Koto-ku, Tokyo 135-18
- 19 0064, Japan
- ⁸ Department of Geosciences, University of Iowa, 10 Glendale Court, Iowa City, IA 52242, USA 20
- ⁹ Geosciences Department, Oregon State University, 128 Kidder Hall, Corvallis, OR 97331, USA 21
- ¹⁰ Japan Agency for Marine-Earth Science and Technology, Natsushima 2-15, Yokosuka 237-22
- 0061, Japan 23

Abstract

| The southernmost Mariana forearc stretched to accommodate opening of the Mariana Trough |
|--|
| backarc basin in late Neogene time, erupting basalts now exposed in the SE Mariana Forearc Rift |
| (SEMFR) 3.7 - 2.7 Ma ago. Today, SEMFR is a broad zone of extension that formed on |
| hydrated, forearc lithosphere and overlies the shallow subducting slab (slab depth $\leq 30 - 50$ km). |
| It comprises NW-SE trending subparallel deeps, 3 - 16 km wide, that can be traced \geq ~ 30 km |
| from the trench almost to the backarc spreading center, the Malaguana-Gadao Ridge (MGR). |
| While forearcs are usually underlain by serpentinized harzburgites too cold to melt, SEMFR crust |
| is mostly composed of Pliocene, low-K basaltic to basaltic andesite lavas that are compositionally |
| similar to arc lavas and backarc basin (BAB) lavas, and thus defines a forearc region that recently |
| witnessed abundant igneous activity in the form of seafloor spreading. SEMFR igneous rocks |
| have low Na ₈ , Ti ₈ , and Fe ₈ , consistent with extensive melting, at $\sim 23 \pm 6.6$ km depth and 1239 \pm |
| 40°C, by adiabatic decompression of depleted asthenospheric mantle metasomatized by slab- |
| derived fluids. Stretching of pre-existing forearc lithosphere allowed BAB-like mantle to flow |
| along SEMFR and melt, forming new oceanic crust. Melts interacted with preexisting forearc |
| lithosphere during ascent. SEMFR is no longer magmatically active and post-magmatic tectonic |
| activity dominates the rift. |

KEYWORDS: forearc rift, seafloor spreading, Mariana arc, subduction zone

1. Introduction

| 47 | Forearcs are cold regions above subduction zones that lie between the trench and the magmatic |
|----|---|
| 48 | arc. They can be accretionary or non-accretionary depending on the amount of sediments carried |
| 49 | into the trench (Lallemand, 2001, Stern, 2002). Non-accretionary forearcs, such as that of the |
| 50 | Marianas, are of special interest as they preserve a record of the first lavas erupted in association |
| 51 | with subduction initiation (Ishizuka et al., 2011, Reagan et al., 2010, Stern & Bloomer, 1992). |
| 52 | Forearc lithosphere is underlain by the cold, subducting plate that releases its hydrous fluids into |
| 53 | the upper mantle wedge, resulting in exceptionally cold (< 400°C; Hulme et al., 2010) and |
| 54 | serpentinized mantle lithosphere that rarely melts (Hyndman & Peacock, 2003, Van Keken et al., |
| 55 | 2002, Wada et al., 2011). The occurrence of cold, serpentinized forearc mantle beneath the |
| 56 | Mariana forearc is demonstrated by eruption of serpentinite mud volcanoes (Hulme et al., 2010, |
| 57 | Mottl et al., 2004, Savov et al., 2007, Savov et al., 2005, Wheat et al., 2008) and serpentinized |
| 58 | peridotite outcroppings on the inner trench slope (Bloomer & Hawkins, 1983, Ohara & Ishii, |
| 59 | 1998). Serpentinized mantle beneath the forearc has also been imaged by geophysical surveys |
| 60 | (Tibi et al., 2008). Ultramafic rocks from the upper mantle wedge found as clasts in mud |
| 61 | volcanoes and on the inner trench slope mostly consist of harzburgite, residues of mantle melting |
| 62 | (Parkinson & Pearce, 1998, Savov et al., 2007, Savov et al., 2005) that are chemically distinct |
| 63 | from the more fertile, backarc basin (BAB) peridotites (Ohara et al., 2002). Such highly depleted |
| 64 | forearc mantle can melt in association with early-arc volcanism to generate boninites (Reagan et |
| 65 | al., 2010, Stern & Bloomer, 1992). Decompression melting of more fertile mantle to form |
| 66 | tholeiitic basalts near the trench also has been documented during the first stage of subduction |
| 67 | initiation. These lavas have MORB-like compositions and have been termed forearc basalts |

(FABs) reflecting their subduction-related origin and location in modern forearcs (Reagan et al.,

69 2010).

In the Izu-Bonin-Mariana (IBM) intraoceanic system, most forearc lavas are Eocene - Oligocene in age and younger forearc lavas are unusual (Ishizuka et al., 2011, Reagan et al., 2010, Stern & Bloomer, 1992). Here, we document the first record of Pliocene forearc lavas from the southernmost Mariana convergent margin, indicating that the mantle can melt beneath forearcs long after subduction initiation. These low-K lavas are tholeitic basalts generated from BAB-like asthenospheric mantle during seafloor spreading in the Southeast Mariana Forearc Rift (SEMFR), which is a broad zone of deformation (~ 40 km wide and ~ 60 km long), extending from the trench to the Fina-Nagu arc Volcanic Chain (FNVC). SEMFR today overlies a shallow subducting Pacific slab (≤ 50 − 100 km deep; Becker, 2005).

This paper presents a first report on the geology and tectonic evolution of the SEMFR. We present bathymetry, summarize the results of bottom traverses, and provide petrologic, major element geochemical data and ⁴⁰Ar/³⁹Ar ages of igneous rocks sampled during two JAMSTEC research cruises. These data are used to characterize SEMFR lavas and to address when, where, and how SEMFR lavas were generated, and to determine sources of the magmas, and conditions of melting. Addressing these issues helps us better understand how such melts were produced in a cold forearc, and allows us to develop a geodynamic model to constrain the geodynamic evolution of the S. Mariana forearc. In this manuscript, we show that SEMFR lavas have BAB-like geochemical and petrographic features; and opening of the Southernmost Mariana Trough allowed adiabatic decompression melting of BAB-like asthenospheric mantle in the forearc to produce SEMFR lavas 3.7 – 2.7 Ma ago.

93

94

95

96

97

98

99

100

101

102

103

104

105

106

107

108

109

110

111

112

113

114

2. Geodynamic setting

The Mariana intraoceanic arc system is the southern third of the IBM convergent margin. It is generally associated with a sediment-starved forearc ~ 200 km wide (Fryer et al., 2003, Kato et al., 2003), submarine and subaerial volcanoes of the active magmatic arc (Baker et al., 2008), and a BAB with a spreading axis that generally lies $\sim 250 - 300$ km from the trench (Stern et al., 2003). Mariana geodynamic evolution was influenced by collisions with buoyant oceanic plateaus (Ogasawara Plateau in the north and Caroline Ridge in the south). These resisted subduction, stimulating backarc extension to open the Mariana Trough between the collisions (Wallace et al., 2005). IBM mostly trends N-S but the southernmost Mariana convergent margin (13°10'N – 11°N) bends to E-W (Fig. 1A; Bird, 2003). This region is deforming rapidly (Kato et al., 2003, Martinez et al., 2000), accompanied by abundant igneous activity. Here, the Mariana Trench reaches the deepest point on Earth at the Challenger Deep (10994 m; Gardner & Armstrong, 2011), and Pacific-Philippine Sea plate convergence is approximately orthogonal to the trench (Bird, 2003). The tectonic evolution of the southernmost Mariana arc began with the Late Miocene collision of the Caroline Ridge, which pinned the Yap arc and allowed the southern Mariana Trough to open, sculpting the southern termination of the arc (Miller et al., 2006b). The southernmost Mariana magmatic arc is poorly developed and entirely submarine, contrasting with the large, often subaerial, arc volcanoes to the north. The arc magmatic front almost intersects the southern end of the BAB spreading center south of 13°N (Fig. 1B; Fryer et al., 2003). These features are about 100 – 150 km from the trench, whereas to the north the BAB spreading axis

lies ~250 – 300 km from the trench and is separated from the magmatic arc by 50 - 100 km (Fryer et al., 1998, Stern et al., 2003). The magmatic arc appears to have been reorganized recently, as evidenced by a complex bathymetric high with multiple nested calderas – an inferred paleo-arc (the Fina-Nagu Volcanic Chain in Fig. 1B) where no hydrothermal activity was observed (Baker et al., 2008) and calderas are covered with sediments (Fig. 1C) - SE of and parallel to the modern magmatic arc (e.g. Toto caldera). The southern Mariana Trough has a well-defined spreading ridge, the Malaguana-Gadao Ridge (MGR), with a well-developed magma chamber and several hydrothermal vents (Baker et al., 2008, Becker et al., 2010, Kakegawa et al., 2008). Because the subducted Pacific plate lies ~ 100 km beneath it, the MGR melt source region captures hydrous fluids usually released beneath arc volcanoes, enhancing mantle melting and resulting in an inflated ridge morphology that is unusually robust for the Mariana Trough backarc basin, in spite of an intermediate spreading rate (< 65 mm/yr; Becker et al., 2010, Fryer et al., 1998, Martinez et al., 2000). More rapid extension along the MGR might also enhance decompression melting (Becker et al., 2010).

The southernmost Mariana convergent margin is underthrust by a narrow slab of Pacific plate (traceable to ~ 250 km depth; Gvirtzman & Stern, 2004), torn N-S at ~ 144°15'E (Fryer et al., 1998, Gvirtzman & Stern, 2004). Analogue experiments show that short, narrow subducted slabs trigger toroidal (around the slab edge) and poloidal (underneath the slab tip) asthenospheric mantle flows that generate rapid slab rollback and trench retreat relative to the upper plate (Funiciello *et al.*, 2003, Funiciello *et al.*, 2006, Schellart *et al.*, 2007). These conditions lead to weak coupling of the subducting plate with the overriding plate, stimulating rapid deformation of the overriding plate (i.e., the southern Mariana Trough) and may be responsible for the very

narrow forearc that defines the southern Mariana margin west of the W. Santa Rosa Bank Fault (Fig. 1B, Gvirtzman & Stern, 2004). The unusual tectonic situation of the southernmost Mariana convergent margin has also affected magmagenesis. Sub-forearc mantle usually is too cold to melt (Van Keken et al., 2002), so that slab-derived fluids only lead to serpentinization (Hyndman & Peacock, 2003, Wada et al., 2011). Instead, the dynamic tectonic setting of the southern Marianas results in mantle melting much closer to the trench than is normally observed.

3. Geology and morphology of the Southeast Mariana Forearc Rift

Most of the IBM convergent margin is underlain by lithosphere that formed after subduction began ~52 Ma (Ishizuka et al., 2011, Reagan et al., 2010). In the southernmost Marianas, Eocene forearc lithosphere was stretched in late Neogene time to accommodate opening of the Mariana Trough BAB; part of this extension is localized along the SEMFR (Martinez & Stern, 2009). The morphological expression of the SEMFR is apparent over a region ~ 40 km wide and at least 60 km long (Supporting Information Table S1.2). SEMFR is composed of broad southeast-trending deeps and ridges (Fig. 1B), each 50 to 60 km long and 3 to 16 km wide, which opened nearly parallel to the trench axis. These rifts can be traced from the Mariana Trench almost to the FNVC (Fig. S1.1 in Supporting Information S1). Eastward, the SEMFR is bounded by a N-S fault, the W. Santa Rosa Bank fault (WSRBF, Fig. 1B; Fryer et al., 2003), which separates thick crust of the broad Eocene forearc to the north and east (including that beneath Santa Rosa Bank) from the deeper and narrower forearc of the S. Marianas - including SEMFR - to the west. WSRBF also appears to overlie a tear in the subducted slab (Fryer et al., 2003, Gvirtzman & Stern, 2004). The WSRBF is taken to be the eastern boundary of the SEMFR because it does not have the same

NNE-SSW trend as the three SEMFR deeps (Fig. 1B), and the forearc is significantly older to the east (Reagan et al., 2010). SEMFR overlies the shallow part of the slab (\leq 30 - 100 km deep, Becker, 2005) and is situated in a region with numerous shallow (crustal) earthquakes, (Martinez & Stern, 2009) signifying active deformation.

164

165

166

167

168

169

170

171

172

173

174

175

176

177

178

179

180

181

182

160

161

162

163

We studied SEMFR by interpreting swathmapped bathymetry and previously published HMR-1 sonar backscatter imagery (Martinez et al., 2000). The region is characterized by high sonar backscatter, indicating little sedimentary cover (Fig. 1C). This was confirmed by Shinkai 6500 manned submersible and YKDT deep-tow camera / dredge seafloor studies. Table S1.1 in Supporting Information S1 summarizes the position and lithologies encountered during these dives (Fig. 1B). Most dives recovered basalt. In addition, deeper crustal and upper mantle lithologies, e.g. diabase, fine-grained gabbros and deformed peridotites, were recovered near the WSRBF (Supporting Information Fig. S1.7 and S1.8). Similar lithologies are also reported by previous studies of the area (Bloomer & Hawkins, 1983, Fryer, 1993, Michibayashi et al., 2009, Sato & Ishii, 2011). Based on relief, the SEMFR can be subdivided along strike into NW, central, and SE sectors. SEMFR relief is ruggedest in the SE sector near the trench, where it is intensely faulted and affected by landsliding, with abundant talus slopes of fragmented basaltic lavas (Fig. 2A, C, D and Fig. S1.5 to S1.8 in Supporting Information). The central SEMFR is less faulted, with more outcrops and less talus, but still has many steep talus slopes and faulted lava flows (Fig. S1.9 - S1.10 in Supporting Information). The NW SEMFR, nearest the MGR, has gentler relief, with better-preserved pillow lava outcrops (Fig. 2B, E and Fig. S1.11 - S1.13 in Supporting Information). We did not recover samples of Paleogene forearc crust in the SEMFR, although this is common to the NE and west, indicating that SEMFR is floored by young, tectonized oceanic

crust. Our bottom observations along with the absence of parallel magnetic fabrics in the SEMFR (Martinez et al., 2000) suggest that the SEMFR is no longer a site of active volcanism.

Toto caldera and part of the MGR near the NW limit of the SEMFR were studied during ROV Kaiko Dives 163 and 164 (R/V Kairei cruise KR00-03 Leg 2, Fig. 1B). Toto caldera, which may be part of the immature magmatic arc, is mostly covered by talus of fresh lava fragments with a whitish coating, perhaps bacteria or sulfur-rich precipitate (Supporting Information Fig. S1.14), derived from the active Nakayama hydrothermal site (Gamo *et al.*, 2004, Kakegawa et al., 2008). The MGR seafloor is mostly composed of fresh, well-preserved pillow lavas alternating with aa and solidified lava lake (Becker et al., 2010), along with active hydrothermal vents (Supporting Information Fig. S1.15) indicating ongoing magmatic activity. Fig. 1C shows high sonar backscatter for Toto caldera and around the MGR, indicating hard rock (fresh lava) exposures and thin sediments, consistent with seafloor seen in dive videos.

4. Methods

Igneous rock samples were collected during two cruises YK08-08 Leg 2 (Shinkai 6500 manned submersible dive 1096) in 2008 and YK10-12 (Shinkai 6500 dives 1230, 1235 and Yokosuka deep-tow camera dredge (YKDT) 85, 86, and 88) in 2010. Representative, fresh samples were selected onboard for petrographic and geochemical studies. Information from Kaiko ROV dives 163 and 164 (R/V Kairei cruise KR00-03 Leg 2 in 2000) is also included. High-resolution videos of the seafloor generated during dives were reviewed during and after the cruises (see Supporting Information S1 for more details). GMT (Smith & Wessel, 1990, Wessel & Smith, 1995b, Wessel & Smith, 1998, Wessel & Smith, 1995a) was used to compile SEMFR bathymetric data,

including swathmapping results from these cruises and those of Gardner (2006), Gardner (2007) and Gardner (2010). Maps were imported into ArcGIS to generate bathymetric cross sections perpendicular to the strike of SEMFR (Fig. S1.1 in Supporting Information).

209

210

211

212

213

214

215

216

217

218

219

220

221

222

223

224

225

226

206

207

208

Igneous rock samples were analyzed, using procedures reported in Supporting Information S2. For major element analyses, fresh sample chips containing as few phenocrysts as possible were hand-picked and powdered in an alumina ball mill. Whole rock chemical analyses for Shinkai dive 1096 samples were carried out on Philips PW1404 X-Ray fluorescence (XRF) spectrometer at the Geological Survey of Japan/AIST. External errors and accuracy are < 2%. Whole rock chemical analyses for other samples were performed at University of Rhode Island by fusion – dissolution of glass beads; and analyses were conducted using a Ultima-C Jobin Yvon Horiba Inductively Coupled Plasma Atomic Emission Spectroscopy (ICP-AES) at Boston University. Glass beads were generated by melting 400 ± 5 mg of lithium metaborate (LiBO₄) flux with 100 ± 5 mg of ignited sample powder at 1050°C for 10 min. Molten beads were dissolved in 5% nitric acid to achieve a final dilution factor of ~ 4000 (Kelley et al., 2003). Calibration curves for ICP-AES data yield $r^2 > 0.999$, reproducibility of replicate analyses are < 3% rsd for each element, and major element oxides sum to 99 ± 1 wt%. Replicates of samples analyzed by ICP-AES and XRF yield averaged reproducibility < 4% rsd for each element. Results are reported in Table 1. For mineralogical chemistry analyses, polished thin sections were prepared for 16 samples. These were analyzed using the Cameca SX-50 electron microprobe at University of Texas at El Paso. Multiple point analyses give a mean value with 1σ precision ≤ 1 wt% for each selected mineral.

Four samples were dated by step-heating ⁴⁰Ar-³⁹Ar at the Geological Survey of Japan/AIST on a VG Isotech VG3600 noble gas mass spectrometer fitted with a BALZERS electron multiplier. Further details of procedures are reported in Supporting Information S2.

231

232

233

5. Results

5.1.Rock description:

234 Here we outline the principal petrographic and mineralogical features of igneous rocks sampled 235 from the SEMFR, Toto caldera and MGR. Method for sample description is reported in 236 Supporting Information S3 and detailed sample descriptions are in Supporting Information S4. 237 SEMFR lavas are mostly aphyric (< 1% phenocrysts) and sparsely phyric (1 - 5% phenocrysts) 238 basalts and basaltic andesites, indicating eruption at near-liquidus temperatures. These are 239 microporphyritic pillows or massive flows, with thin, microcrystallite-rich glassy rims (1 - 11 mm)240 of fresh, translucent to dark brown glass), thin (≤ 1 mm) Mn coat, and negligible alteration (Fig. 241 3). Pillow lavas are vesicular despite being collected at $\sim 6000 - 3000$ m, indicating that these 242 magmas contained significant volatiles. In contrast, basalt massive lava flows are more crystalline 243 and less vesicular. Embayed phenocrysts indicate disequilibrium, perhaps due to magma mixing. 244 Pillowed lavas sampled in the NW (YKDT-88) contain larger crystals (≥ 0.5 mm) of 245 clinopyroxene and olivine set in a finely microcrystalline olivine-rich groundmass (Fig. 3C). 246 Similar olivine-rich lavas were not sampled elsewhere in the SEMFR. Diabase and fine-grained 247 gabbros were also recovered near the WSRB fault (Shinkai 6500 dive 1235; Fig. 3B, D). These 248 might represent the lower crust of SEMFR (dike complex and gabbro layer). Pillow lavas from 249 MGR are very fresh, with translucent glassy rinds. Lavas are vesicular, cryptocrystalline 250 andesites with a glassy groundmass and <1% plagioclase microlites. Lava flows from Toto

caldera are vesicular, sparsely phyric to aphyric, fine-grained to cryptocrystalline basaltic andesites.

253

254

255

256

257

258

259

260

261

262

263

264

265

266

267

268

269

270

271

272

273

251

252

5.2. Major element and mineral compositions:

SEMFR lavas are fresh basalts and basaltic andesites, with 50.4 to 57.0 wt% SiO₂ (data reported are adjusted to 100% total on an anhydrous basis, Fig. 4A). In terms of normative compositions, all lavas are quartz tholeiites. These define a low-K to medium-K suite, with $K_2O < 1$ wt%. Lava compositions cluster along the tholeiitic – calc-alkaline boundary on a plot of FeO*/MgO vs. SiO₂ (Fig. 4B; Miyashiro, 1974), or along the medium-Fe / low-Fe boundary (Arculus, 2003). Lavas recovered during Shinkai 6500 dive 1096 and 1230 and YKDT-86 and -88 are relatively primitive, with whole-rock Mg# (= atomic Mg * 100 / (Mg + Fe)) > 60, Fig. 4C). Other SEMFR samples are significantly more fractionated, with Mg# = 41 - 60. Composition of SEMFR lavas is reported in Table 1. MGR and Toto caldera lavas are mostly andesites ($SiO_2 = 55.1 - 61.7$ wt%, with $K_2O < 0.5$ wt% and Mg# = 33 – 53). None of the studied lavas are boninitic (MgO > 8 wt%, $SiO_2 > 52$ wt%, $TiO_2 < 0.5$ wt%; Le Bas, 2000). Toto caldera lavas plot within the compositional field of southernmost Mariana volcanic arc lavas (SMA: 13°10'N – 11°N, Kakegawa et al., 2008, Stern et al., 2013), suggesting that Toto caldera belongs to the S. Mariana arc volcanoes (SMA). Toto caldera samples also cluster along the tholeitic – calc-alkaline boundary. In contrast, MGR lavas are tholeiitic (medium-Fe to high-Fe) basaltic andesites and andesites (Kakegawa et al., 2008, Pearce et al., 2005; Fig. 4A, B). The Fe enrichment of the MGR lavas (Fig. 4B) suggests that their parental magmas contain less water, inhibiting early crystallization of Fe-oxides. In Fig. 4A, MGR lavas do not plot along the SEMFR fractionation trend, and their similar K₂O content suggests that MGR and SEMFR lavas interacted with similar arc-like slab-derived fluids. FABs

(Reagan et al., 2010) are low-K to medium-K basalt to basaltic andesites that plot within the tholeiitic and calc-alkaline fields (Fig. 4B, C); and SEMFR plot along the FAB fractional trend (Fig. 4C, D). All lavas from the southernmost Marianas suggest fractionation controlled by plagioclase, clinopyroxene ± olivine crystallization trend (Fig. 4C, F).

278

279

280

281

282

283

284

285

286

287

288

289

290

291

292

293

274

275

276

277

SEMFR basalts and basaltic andesites contain olivine, clinopyroxene, and plagioclase. Results for representative mineral composition are listed in Supporting Information Tables S4.1 to S4.4 and summarized in Table 2. Mineral compositions correlate with whole rock chemical compositions (Fig. 5A, B and Supporting Information S5). Near-primitive (Mg# > 60), olivine-rich SEMFR lavas (Shinkai dive 1096, upper series and YKDT-88) contain Mg-rich olivines (Fo₈₆₋₈₈) in equilibrium with Mg-rich clinopyroxene (Mg# = 83 - 91) and anorthitic plagioclase (An ≥ 80). In contrast, fractionated (Mg# \leq 60) lavas have Fe-rich olivine (Fo₇₅₋₈₄) coexisting with two kinds of clinopyroxene (endiopside – diopside with Mg $\# \ge 80$ and augite with Mg# < 80) and plagioclase (An \geq 80 and An < 80). Reverse and oscillatory zoning is only observed in more fractionated plagioclase (An < 80 in the core), suggesting magma mixing perhaps in a magmatic reservoir. Fine-grained gabbro and diabase have Mg-rich clinopyroxenes (Mg# \geq 60) coexisting with more albitic plagioclase (An \leq 70). The mineral composition of Toto caldera lavas and MGR lavas are within the compositional range of SEMFR lavas. Occurrence of two mineral compositional groups in Toto and MGR lavas, without significant compositional overlap, strongly suggests magma mixing (Supporting Information S4.2 and Fig. S4.1).

294

295

296

297

Olivine xenocrysts (≥ 0.5 mm) enclosing chromium spinel are common in primitive lavas (Fig. 3C, 5E). Olivine xenocrysts have higher Fo contents (Fo₈₉₋₉₂ core and Fo₈₇₋₉₇ rim) than do the olivine phenocrysts (Fo₈₆₋₈₈, Table S4.3 and Fig. S4.1 in Supporting Information) in their host

basalts. Olivine xenocrysts host chromium spinel with Cr# (= 100 x Cr / (Cr+Al)) = 47 – 73. The olivine – spinel assemblages plot in the mantle array of Arai (1994) and they are similar to those of the SE Mariana forearc mantle peridotite (Cr# > 50 and Fo_{90-92} , Ohara & Ishii, 1998), suggesting that these xenocrysts are samples of forearc mantle (Fig. 5C).

303 5.3. ⁴⁰Ar-³⁹Ar ages:

Four SEMFR samples (2 samples from Shinkai 6500 dive 1096, 1 sample each from Shinkai 6500 dive 1230 and YKDT-88) were dated by step-heating 40 Ar- 39 Ar (Fig. 6 and Table 1). Initial 40 Ar/ 36 Ar for these samples (290 - 295) is nearly atmospheric (40 Ar/ 36 Ar $_{atmosphere}$ = 298.6), indicating that negligible radiogenic 40 Ar was inherited. Dated samples from dive 1096 samples include one from each of the lower (1096-R2) and upper series (1096-R16) lavas. These gave indistinguishable plateau ages of 3.5 ± 0.4 Ma (lower series 1096-R2) and 3.7 ± 0.3 Ma (upper series 1096-R16). Shinkai dive 1230 and YKDT-88 gave slightly younger ages, respectively of 2.8 ± 0.5 Ma and 2.7 ± 0.3 Ma. SEMFR 40 Ar- 39 Ar ages indicate that seafloor spreading occurred in Pliocene time (Fig. 1B), and suggests that SEMFR seafloor youngs toward the MGR.

6. Discussion

6.1. Genesis of SEMFR lavas:

Compositions of lavas and their minerals record the conditions of magma genesis and evolution; and from this, important tectonic information can be gleaned (e.g. Klein & Langmuir, 1987). Incompatible elements such as K₂O, Na₂O and TiO₂ are concentrated in the melt as mantle melting or crystal fractionation proceeds. The first melt fraction is enriched in these elements and

so concentrations anti-corrrelate with fraction of melting, or "F" (Kelley et al., 2006, Kelley et al., 2010, Klein & Langmuir, 1987, Taylor & Martinez, 2003). In addition, K₂O contents in convergent margin magma sources are strongly affected by subduction-related metasomatism (e.g. K-h relationship, Dickinson, 1975, Kimura & Stern, 2008), therefore this element is generally not used to monitor F. FeO contents in basalts also contain petrogenetic information. In basaltic systems, deeper melts are progressively enriched in iron (Klein & Langmuir, 1987). Therefore, the Na₂O, TiO₂ and FeO contents of lavas are good proxies for the degree and depth of melting. However, estimating the extent and depth of partial melting requires primitive lavas with compositions in equilibrium with their mantle source; consequently, Na₂O, TiO₂ and FeO contents are commonly corrected for olivine fractionation in order to infer their Na₈, Ti₈ and Fe₈ contents (Na₂O, TiO₂ and FeO contents calculated at MgO = 8 wt%). The Na₈ of N-MORBs anticorrelates with Fe₈, indicating that melting is greater if it begins deeper (Fig. 7A; Arevalo Jr. & McDonough, 2010, Klein & Langmuir, 1987). Subduction-related melting is somewhat different because melting extents are enhanced by water (Gribble et al., 1996, Kelley et al., 2006, Taylor & Martinez, 2003). BAB magma sources often are affected by subducted water and are characterized by more melting at shallower depth than MORBs, so that Na₈ increases with Fe₈ (Fig. 7A; Kelley et al., 2006, Taylor & Martinez, 2003). BAB and arc lavas have distinct geochemical signatures (Fig. 7), resulting from elements dissolved in fluids derived from the subducting slab that are involved in magma genesis. Arc lavas have lower Na₈ and Ti₈ contents at higher K₂O/TiO₂ and Fe₈ content because they formed by high degrees of melting at greater depths in the presence of slab-derived fluids. In contrast, BAB lavas have higher Na₈ and Ti₈ contents at lower K₂O/TiO₂ and Fe₈ content, as they were generated at shallower depth by adiabatic mantle decompression, with less involvement of slab-derived fluids.

320

321

322

323

324

325

326

327

328

329

330

331

332

333

334

335

336

337

338

339

340

341

344 To investigate SEMFR magmagenesis (i.e. whether SEMFR lavas were produced in a BAB-like 345 and / or in a arc-like magmagenetic settings), we calculated Na₈, Ti₈ and Fe₈ contents for these 346 lavas. Plots of Al₂O₃, CaO and FeO* against MgO (Fig. 4D-F) show that the kinks in Al₂O₃ and 347 CaO, indicating the beginning of plagioclase and clinopyroxene crystallization, are respectively 348 observed at MgO = 6 wt% and at MgO \sim 7 wt%. Therefore, data were filtered to exclude highly 349 fractionated samples with MgO < 7 wt% that crystallized olivine, clinopyroxene and plagioclase 350 on their LLD (Fig. 4D-F), following the method described in Kelley et al. (2006) and Kelley et al. 351 (2010). The least fractionated samples with 7 - 8 wt% MgO, which fractionated oliving only (Fig. 352 4D-F), were then corrected to MgO = 8 wt% using the equations of Klein and Langmuir (1987) 353 for Na₈ and Fe₈, and Taylor and Martinez (2003) for Ti₈. These are listed in Table 1 (mean 354 SEMFR Na₈ = 1.99 \pm 0.40 wt% (1 std. dev.); mean Ti₈ = 0.60 \pm 0.11 wt%; mean Fe₈ = 6.91 \pm 355 0.54 wt%). The Na₈ Fe₈ and Ti₈ contents of SEMFR lavas are slightly lower than those 356 observed for N-MORBs (Arevalo Jr. & McDonough, 2010), indicating higher degrees of mantle 357 melting produced shallower. SEMFR lavas have similar Ti₈ and Na₈ contents at lower Fe₈ than 358 FABs; and they plot in the compositional overlap between Mariana arc lavas and the Mariana 359 BAB lavas, with homogeneous, low Na₈ and Ti₈ contents varying little with Fe₈ content (Fig. 7A 360 - B), suggesting a roughly constant degree and depth of mantle melting. These lavas were 361 produced by extensive melting ($\geq 15\%$) of shallow mantle ($\sim 25 \pm 6.6$ km, see section 6.2). The 362 K₂O/TiO₂ (proxy for the total subduction input; Shen & Forsyth, 1995) of SEMFR lavas is higher 363 that of FABs and plot between the arc – BAB compositional fields (Fig. 7C - D), well above N-364 MORBs, further demonstrating a subduction component in SEMFR magma genesis. Only lavas 365 from YKDT-88, collected closest to the FNVC (Fig. 1B), do not plot on the SEMFR 366 compositional field (Fig. 7A-C), with lower Na₈ and Ti₈ at similar Fe₈ contents. Their Ti₈ and Na₈ 367 values are lower than those of Mariana arc lavas (Fig. 7A-C), suggesting that YKDT-88 lavas

were produced by more mantle melting and / or melting of a more depleted mantle source at similar depth compared to other SEMFR magmas.

370

371

372

373

374

375

376

377

378

379

380

381

382

383

384

385

386

368

369

The above inference that SEMFR lavas are similar to back-arc basin basalts (BABB) can be checked by examining mineral compositions, because arc basalts and BABBs have distinct An-Fo relationships (Stern, 2010). Arc basalts contain more Fe-rich olivine with more An-rich plagioclase compared to BABB, MORB, and OIB (Ocean Island Basalt, Fig. 8A) because higher water contents in arc magmas delay plagioclase but not olivine crystallization (Kelley et al., 2010, Stern, 2010), resulting in higher CaO and FeO contents in the melt when plagioclase starts crystallizing. In contrast, BABBs, formed largely by adiabatic decompression mantle melting, have Fo-An relationships essentially indistinguishable from those of MORB and OIB (Fig. 8A). Accordingly, we can discriminate arc basalts from BABBs based on An and Fo contents of the plagioclase – olivine assemblages. Fig. 8A shows that most SEMFR lavas plot within the BABB compositional field, consistent with observations from Na₈, Ti₈, and Fe₈ discussed in the previous section. Some samples also plot within the arc compositional field, strongly suggesting that BABlike (i.e. adiabatic decompression melting) and arc-like (i.e. wet mantle melting) conditions of magmagenesis coexisted beneath SEMFR. We propose that SEMFR magmas formed by adiabatic decompression of fertile asthenospheric mantle (BAB-like mantle) metasomatized by slabderived fluids, enriching the melt in water and sometimes delaying plagioclase fractionation.

387

388

389

390

6.2.Pressure and temperature of mantle melting:

The P-T conditions of mantle melting, recorded by primary melts in equilibrium with the mantle beneath SEMFR, were calculated from major element compositions of primitive basalts with 391 MgO \geq 7 wt% (Kelley et al., 2010; Fig. 4D-F) by using the geothermobarometer of Lee *et al.* 392 (2009), based on Si, Mg and water contents of primitive magmas. The estimated P-T conditions 393 are those of the last melt in equilibrium with the mantle or a mean value of the P-T conditions of 394 polybaric, fractional pooled melts recorded along a melting column (Kelley et al., 2010). SEMFR 395 lavas are compositionally similar to BABBs, we therefore used BAB-like oxidation state 396 (Fe³⁺/Fe_T= 0.17) and averaged Mariana BAB water content (1.31 wt%; Gribble et al., 1996, Kelley & Cottrell, 2009) for SEMFR lavas, Fe³⁺/Fe_T = 0.17 for Mariana Trough lavas and 397 398 Fe³⁺/Fe^T = 0.25 for Mariana arc magmas (Kelley & Cottrell, 2009). We also used lherzolitic 399 BAB-like mantle source (Fo₉₀; Kelley et al., 2006) to estimate the P-T conditions of SEMFR 400 mantle melting. Primitive lavas of the Mariana Trough and the Mariana arc with analyzed water 401 were filtered for MgO > 7 wt % as SEMFR lavas for consistency. SEMFR whole rock 402 compositions indicate melting pressures of 0.5 - 0.9 GPa (± 0.2 GPa) and temperatures of 1217 -403 1269° C ($\pm 40^{\circ}$ C), with a mean of 0.7 ± 0.2 GPa ($\sim 23 \pm 6.6$ km) and $1239 \pm 40^{\circ}$ C (Fig. 8B). This 404 is consistent with melting just above the present subducting slab ($\leq 30-100$ km depth), although 405 we do not know the position of the subducting slab at 2.7 - 3.7 Ma, when SEMFR melts were 406 generated. Mariana Trough BABBs (Gribble et al., 1996, Kelley & Cottrell, 2009) have similar P-407 T conditions of mantle melting $(0.7 - 1.5 \pm 0.2 \text{ GPa}, 1214 - 1359 \pm 40^{\circ}\text{C};$ mean melting depth ~ 408 33 ± 6.6 km). In contrast, Mariana arc lavas (Kelley et al., 2010, Shaw et al., 2008) show higher 409 P-T conditions of mantle melting $(1.1 - 3.0 \pm 0.2 \text{ GPa}, 1240 - 1522 \pm 40^{\circ}\text{C})$. These results 410 suggest that SEMFR lavas and Mariana Trough BABBs were similarly generated by adiabatic 411 decompression of shallow asthenospheric mantle ($\sim 25-30\pm 6.6$ km). In contrast, arc lavas 412 (Kelley & Cottrell, 2009, Kelley et al., 2010, Shaw et al., 2008) recorded deeper (mean melting 413 depth $\sim 51 \pm 6.6$ km), and hotter mantle melting conditions (Kelley et al., 2010). This leads to the 414 further deduction that SEMFR lavas formed by BABB-like seafloor spreading at 2.7 to 3.7 Ma.

6.3. Geodynamic evolution of the Southeastern Mariana Forearc Rift:

Investigations of the petrography and geochemistry of SEMFR lavas reveal that i) SEMFR lavas are petrographically and compositionally similar to Mariana Trough BABBs; ii) SEMFR melts interacted with the pre-existing forearc lithosphere and picked up some forearc mantle olivines, indicating rapid ascent; iii) magmatic activity (2.7 – 3.7 Ma) formed SEMFR oceanic crust by seafloor spreading (no Eocene forearc basement has been recovered from the SEMFR); iv) SEMFR primitive basalts formed by decompression melting at ~ 23 km depth and 1239°C, like that associated with the Mariana Trough backarc basin, suggesting similar formation; and v) lack of evidence for recent igneous and hydrothermal activity, except near MGR and Toto caldera, indicates that the presently-observed NNW-SSE trending relief formed during post-magmatic rifting (< 2.7 Ma).

SEMFR is a rift with no morphological expression of large arc-like volcanoes, like those of the Mariana arc. SEMFR lavas are vesicular with K₂O contents (Fig. 4A) and K₂O/TiO₂ ratios that are similar to MGR and other Mariana Trough BAB lavas (Fig. 7C, D). They also have similar P-T conditions of magma genesis, demonstrating that they formed by adiabatic decompression of BAB-like mantle metasomatized by slab-derived fluids. These observations raise a fundamental question: were SEMFR lavas produced by seafloor spreading in the backarc basin or in the forearc? The southernmost Mariana convergent margin has reorganized rapidly since its collision with the Caroline Ridge, suggesting that SEMFR lavas were produced by different geological settings that what exists today. From the location of SEMFR adjacent to the trench, it is clear that these lavas formed in the forearc. We propose a geodynamic model for the southernmost Mariana

arc, in which SEMFR formed to accommodate opening of the southernmost Mariana Trough (Fig. 9A, B and Fig. 10A-C). Rupturing the forearc lithosphere allowed asthenospheric mantle to flow into the forearc and to melt by adiabatic decompression under hydrous conditions 2.7 - 3.7 Ma ago; and origin of SEMFR mantle (i.e. from the backarc basin, the arc or a slab window) is still under investigation. Some SEMFR melts picked up fragments of pre-existing forearc mantle during ascent, demonstrating that SEMFR lavas formed long after subduction initiation. Post-magmatic activity (< 2.7 Ma ago) shapes the S. Mariana forearc lithosphere (Fig. 9C) and formed the NNW-SSE trending rifts of SEMFR, as we know it today (Fig. 9D and Fig. 10D).

7. Conclusions

Two important conclusions can be drawn from this study: i) SEMFR magmas formed by adiabatic decompression in the southernmost IBM forearc, usually underlain by cold, serpentinized harzburgitic mantle that rarely melts (Reagan et al., 2010); and ii) SEMFR lavas were produced by melting of fertile asthenospheric mantle metasomatized by slab-derived fluids, long after subduction initiation, allowing development of a forearc lithosphere. Our results show that the southernmost Mariana forearc stretched to accommodate opening of the Mariana Trough to form the SEMFR, allowing hydrated, asthenospheric mantle to flow into the forearc and to produce new oceanic crust $\sim 2.7-3.7$ Ma ago. SEMFR lavas formed by adiabatic decompression of depleted backarc mantle at $\sim 30\pm 6.6$ km depth and $1224\pm 40^{\circ}$ C. SEMFR at 2.7-3.7 Ma was likely a ridge-like spreading center, where the slab-derived fluids enhanced mantle melting beneath the forearc. Today, SEMFR is no longer magmatically active and amagmatic extension shapes its morphology.

Acknowledgements

We thank JAMSTEC for providing Kaiko samples and related videos, Teruaki Ishii, Stuart Murchison, Katsuyoshi Michibayashi, Warren Lieu, Susumu Umino and two anonymous reviewers for their help and their insightful comments that improved this manuscript. Many thanks to the R/V Yokosuka crew for their efforts work during YK08-08 Leg 2 and YK10-12 cruises. This research was supported by NSF grant 0961352 to RJS. This is UTD Geosciences Contribution # 1246.

| 468 469 | ARAI S. 1994. Characterization of spinel peridotites by olivine-spinel compositional relationships: Review and interpretation. <i>Chemical Geology</i> 113, 191-204. |
|--------------------------|--|
| 470 471 | ARCULUS R. J. 2003. Use and abuse of the terms calcalkaline and calcalkalic. <i>Journal of petrology</i> 44, 929-935. |
| 472 473 | AREVALO JR. R. & MCDONOUGH W. F. 2010. Chemical variations and regional diversity observed in MORB. <i>Chemical Geology</i> 271, 70-85. |
| 474 475 476 | BAKER E. T., EMBLEY R. W., WALKER S. L. <i>et al.</i> 2008. Hydrothermal activity and volcano distribution along the Mariana arc. <i>Journal of Geophysical Research</i> 113, B08S09, DOI: 10.1029/2005GC000948. |
| 477 478 | BECKER N. C. 2005. Recent volcanic and tectonic evolution of the southern Mariana arc. <i>PhD thesis</i> , pp. 166, University of Hawai'i, Hawai'i. |
| 479 480 481 | BECKER N. C., FRYER P. & MOORE G. F. 2010. Malaguana-Gadao Ridge: Identification and implications of a magma chamber reflector in the southern Mariana Trough. Geochemistry Geophysics Geosystems 11, Q04X13, DOI: 10.1029/2009GC002719. |
| 482 483 | BIRD P. 2003. An updated digital model of plate boundaries. <i>Geochemistry Geophysics Geosystems</i> 4, 1027, DOI:10.1029/2001GC000252. |
| 484 485 486 487 | BLOOMER S. H. & HAWKINS J. W. 1983. Gabbroic and ultramafic rocks from the Mariana Trench: An island arc ophiolite. <i>In</i> Hayes D. E. (ed.) <i>The Tectonic and Geologic Evolution of Southeast Asian Seas and Islands: Part 2.</i> American Geophysical Union, Geophysical Monograph Series 27, pp. 294-317, Washington, D.C. |
| 488 489 | DICKINSON W. R. 1975. Potash-Depth (K-h) Relations in Continental Margin and Intra- Oceanic Magmatic Arcs. <i>Geology</i> 3, 53-56. |
| 490 491 492 | FRYER P. 1993. The relationship between tectonic deformation, volcanism, and fluid venting in the southeastern Mariana convergent plate margin. <i>Proceedings of Jamstec, Symposium on deep sea research</i> 9, 161–179. |
| 493 494 | FRYER P., BECKER N., APPELGATE B., MARTINEZ F., EDWARDS M. & FRYER G. 2003. Why is the Challenger Deep so deep? <i>Earth and Planetary Science Letters</i> 211, 259-269. |
| 495 496 497 | FRYER P., FUJIMOTO H., SEKINE M. <i>et al.</i> 1998. Volcanoes of the southwestern extension of the active Mariana island arc: new swath-mapping and geochemical studies. <i>Island Arc</i> 7, 596-607. |
| 498 499 500 | FUNICIELLO F., FACCENNA C., GIARDINI D. & REGENAUER-LIEB K. 2003. Dynamics of retreating slabs: 2. Insights from three-dimensional laboratory experiments. <i>Journal of Geophysical Research</i> 108, 2207, DOI: 10.1029/2001JB000896. |

| 501 502 503 504 | FUNICIELLO F., MORONI M., PIROMALLO C., FACCENNA C., CENEDESE A. & BUI H. A. 2006. Mapping mantle flow during retreating subduction: Laboratory models analyzed by feature tracking. <i>Journal of Geophysical Research</i> 111, B03402, DOI: 10.1029/2005JB003792. |
|--------------------------|---|
| 505 506 507 | GAMO T., MASUDA H., YAMANAKA T. <i>et al.</i> 2004. Discovery of a new hydrothermal venting site in the southernmost Mariana Arc: Al-rich hydrothermal plumes and white smoker activity associated with biogenic methane. <i>Geochemical Journal</i> 38, 527-534. |
| 508 509 510 511 | GARDNER J. V. 2006. Law of the Sea Cruise to Map the Western Insular Margin and 2500-m Isobath of Guam and the Northern Mariana Islands. Cruise report. <i>Center for Coastal and Ocean Mapping (CCOM)/Joint Hydrographic Center (JHC)</i> , University of New Hampshire (UNH), Durham, NH. |
| 512 513 514 515 | GARDNER J. V. 2007. U.S. Law of the Sea Cruise to Map the Western Insular Margin and 2500-m Isobath of Guam and the Northern Mariana Islands. Cruise report. <i>Center for Coastal and Ocean Mapping (CCOM)/Joint Hydrographic Center (JHC)</i> , University of New Hampshire (UNH), Durham, NH. |
| 516 517 518 519 | GARDNER J. V. 2010. U.S. Law of the Sea cruises to map sections of the Mariana Trench and the eastern and southern insular margins of Guam and the Northern Mariana Islands. Cruise report. <i>Center for Coastal and Ocean Mapping (CCOM)/Joint Hydrographic Center (JHC)</i> , University of New Hampshire (UNH), Durham, NH. |
| 520 521 522 | GARDNER J. V. & ARMSTRONG A. A. 2011. The Mariana Trench: A new view based on multibeam echosounding. <i>American Geophysical Union, Fall Meeting 2011</i> , abstract #OS13B-1517, San Fransisco. |
| 523 524 525 526 | GRIBBLE R. F., STERN R. J., BLOOMER S. H., STÜBEN D., O'HEARN T. & NEWMAN S. 1996. MORB mantle and subduction components interact to generate basalts in the southern Mariana Trough back-arc basin. <i>Geochimica et Cosmochimica Acta</i> 60, 2153-2166. |
| 527 528 529 | GVIRTZMAN Z. & STERN R. J. 2004. Bathymetry of Mariana trench-arc system and formation of the Challenger Deep as a consequence of weak plate coupling. <i>Tectonics</i> 23, TC2011, DOI: 10.1029/2003tc001581. |
| 530 531 532 | HAWKINS J. W., LONSDALE P. F., MACDOUGALL J. D. & VOLPE A. M. 1990. Petrology of the axial ridge of the Mariana Trough backarc spreading center. <i>Earth and Planetary Science Letters</i> 100, 226-250. |
| 533 534 535 | HULME S. M., WHEAT C. G., FRYER P. & MOTTL M. J. 2010. Pore water chemistry of the Mariana serpentinite mud volcanoes: A window to the seismogenic zone. <i>Geochemistry Geophysics Geosystems</i> 11, Q01X09, DOI:10.1029/2009gc002674. |
| 536 537 | HYNDMAN R. D. & PEACOCK S. M. 2003. Serpentinization of the forearc mantle. <i>Earth and Planetary Science Letters</i> 212, 417-432. |

| 538 539 540 | ISHIZUKA O., TANI K., REAGAN M. K. <i>et al.</i> 2011. The timescales of subduction initiation and subsequent evolution of an oceanic island arc. <i>Earth and Planetary Science Letters</i> 306, 229-240. |
|--------------------------|---|
| 541 542 | JAQUES A. L. & GREEN D. H. 1980. Anhydrous melting of peridotite at 0–15 Kb pressure and the genesis of tholeitic basalts. <i>Contributions to Mineralogy and Petrology</i> 73, 287-310. |
| 543 544 545 | KAKEGAWA T., UTSUMI M. & MARUMO K. 2008. Geochemistry of Sulfide Chimneys and Basement Pillow Lavas at the Southern Mariana Trough (12.55°N and 12.58°N). <i>Resource Geology</i> 58, 249-266. |
| 546 547 548 | KATO T., BEAVAN J., MATSUSHIMA T., KOTAKE Y., CAMACHO J. T. & NAKAO S. 2003. Geodetic evidence of back arc spreading in the Mariana trough. <i>Geophysical Research Letters</i> 30, 1625, DOI:10.1029/2002GL016757. |
| 549 550 551 | KATZ R. F., SPIEGELMAN M. & LANGMUIR C. H. 2003. A new parameterization of hydrous mantle melting. <i>Geochemistry Geophysics Geosystems</i> 4, 1073, DOI: 10.1029/2002GC000433. |
| 552 553 | KELLEY K. A. & COTTRELL E. 2009. Water and the Oxidation State of Subduction Zone Magmas. <i>Science</i> 325, 605-607. |
| 554 555 556 | KELLEY K. A., PLANK T., GROVE T. L., STOLPER E. M., NEWMAN S. & HAURI E. 2006. Mantle melting as a function of water content beneath back-arc basins. <i>Journal of Geophysical Research</i> 111, B09208, DOI: 10.1029/2005jb003732. |
| 557 558 559 | KELLEY K. A., PLANK T., LUDDEN J. & STAUDIGEL H. 2003. Composition of altered oceanic crust at ODP Sites 801 and 1149. <i>Geochemistry Geophysics Geosystems</i> 4, 8910, DOI: 10.1029/2002GC000435. |
| 560 561 | KELLEY K. A., PLANK T., NEWMAN S. <i>et al.</i> 2010. Mantle Melting as a Function of Water Content beneath the Mariana Arc. <i>Journal of Petrology</i> 51, 1711-1738. |
| 562 563 564 565 | KIMURA JI. & STERN R. J. 2008. Neogene Volcanism of the Japan Island Arc: The K-h Relationship Revisited. <i>In</i> Spencer J.E. and Titley S.R. (ed.) Ores and Orogenesis; <i>Circum-Pacific Tectonics, Geologic Evolution, and Ore Deposits</i> . Geological Society, Digest 22, pp., 187-202, Arizona. |
| 566 567 | KLEIN E. M. & LANGMUIR C. H. 1987. Global correlations of ocean ridge basalt chemistry with axial depth and crustal thickness. <i>Journal of Geophysical Research</i> 92, 8089-8115. |
| 568 569 | LALLEMAND S. 2001. <i>La subduction océanique</i> , Gordon and Breach Science Publishers, Amsterdam. |
| 570 571 | LE BAS M. J. 2000. IUGS Reclassification of the High-Mg and Picritic Volcanic Rocks. <i>Journal of Petrology</i> 41, 1467-1470. |

| 572573574575 | LEE CT. A., LUFFI P., PLANK T., DALTON H. & LEEMAN W. P. 2009. Constraints on the depths and temperatures of basaltic magma generation on Earth and other terrestrial planets using new thermobarometers for mafic magmas. <i>Earth and Planetary Science Letters</i> 279, 20-33. |
|---|---|
| 576 577 | MARTINEZ F., FRYER P. & BECKER N. 2000. Geophysical characteristics of the southern Mariana Trough, 11°50'N-13°40'N. <i>Journal of Geophysical Research</i> 105, 16,591-16,607. |
| 578 579 580 | MARTINEZ F. & STERN R. J. 2009. The Southern Mariana Convergent Margin: A Pre- Ophiolite Analogue. <i>American Geophysical Union, Fall Meeting 2009</i> , abstract#T33D- 05, San Fransisco. |
| 581 582 583 584 | MICHIBAYASHI K., OHARA Y., STERN R. J. et al. 2009. Peridotites from a ductile shear zone within back-arc lithospheric mantle, southern Mariana Trench: Results of a Shinkai 6500 dive. <i>Geochemistry Geophysics Geosystems</i> 10, Q05X06, DOI: 10.1029/2008GC002197. |
| 585 586 587 | MILLER M. S., GORBATOV A. & KENNETT B. L. N. 2006a. Three-dimensional visualization of a near-vertical slab tear beneath the southern Mariana arc. <i>Geochemistry Geophysics Geosystems</i> 7, Q06012, DOI:10.1029/2005gc001110. |
| 588 589 590 | MILLER M. S., KENNETT B. L. N. & TOY V. G. 2006b. Spatial and temporal evolution of the subducting Pacific plate structure along the western Pacific margin. <i>Journal of Geophysical Research</i> 111, B02401, DOI: 10.1029/2005jb003705. |
| 591 592 | MIYASHIRO A. 1974. Volcanic rock series in island arcs and active continental margins. <i>American Journal of Science</i> 274, 321-355. |
| 593 594 595 | MOTTL M. J., WHEAT C. G., FRYER P., GHARIB J. & MARTIN J. B. 2004. Chemistry of springs across the Mariana forearc shows progressive devolatilization of the subducting plate. <i>Geochimica et Cosmochimica Acta</i> 68, 4915-4933. |
| 596 597 | OHARA Y. & ISHII T. 1998. Peridotites from the southern Mariana forearc: Heterogeneous fluid supply in mantle wedge. <i>Island Arc</i> 7, 541-558. |
| 598 599 600 601 | OHARA Y., REAGAN M., ISHII T. <i>et al.</i> 2008. R/V Yokosuka YK08-08 LEG 2 cruise report: Structure and origin of the Mariana forearc and implications for the origin of the continental crust: A Shinkai 6500 study of he southern Mariana forearc. JAMSTEC, Yokosuka. |
| 602 603 | OHARA Y., REAGAN M., MICHIBAYASHI K. <i>et al.</i> 2010. R/V Yokosuka YK10-12 cruise report: Composition, tectonic and structure of the Mariana forearc. JAMSTEC, Yokosuka. |
| 604 605 606 | OHARA Y., STERN R. J., ISHII T., YURIMOTO H. & YAMAZAKI T. 2002. Peridotites from the Mariana Trough: first look at the mantle beneath an active back-arc basin. <i>Contributions to Mineralogy and Petrology</i> 143, 1-18. |

- 607 PARKINSON I. J. & PEARCE J. A. 1998. Peridotites from the Izu-Bonin-Mariana Forearc 608 (ODP Leg 125): Evidence for Mantle Melting and Melt-Mantle Interaction in a Supra-609 Subduction Zone Setting. *Journal of petrology* 39, 1577-1618. 610 PEARCE J. A., STERN R. J., BLOOMER S. H. & FRYER P. 2005. Geochemical mapping of the 611 Mariana arc-basin system: Implications for the nature and distribution of subduction 612 components. Geochemistry Geophysics Geosystems 6, 27, DOI:10.1029/2004GC000895. 613 PECCERILLO A. & TAYLOR S. R. 1976. Geochemistry of Eocene calcalkaline volcanic rocks 614 from the Kastamonu Area, Northern Turkey. Contributions to Mineralogy and Petrology 615 58, 63-81. 616 REAGAN M. K., ISHIZUKA O., STERN R. J. et al. 2010. Fore-arc basalts and subduction 617 initiation in the Izu-Bonin-Mariana system. Geochemistry Geophysics Geosystems 11, 618 Q03X12, DOI: 10.1029/2009GC002871. 619 ROEDER P. L. & EMSLIE R. F. 1970. Olivine-liquid equilibrium. Contributions to Mineralogy 620 and Petrology 29, 275-289. 621 RÜPKE L. H., MORGAN J. P., HORT M. & CONNOLLY J. A. D. 2004. Serpentine and the 622 subduction zone water cycle. Earth and Planetary Science Letters 223, 17-34. 623 SATO H. & ISHII T. 2011. Petrology and Mineralogy of Mantle Peridotites from the Southern 624 Marianas. In Ogawa Y., Anma R. and Dilek Y. (ed.) Accretionary Prisms and Convergent 625 Margin Tectonics in the Northwest Pacific Basin, Modern Approaches in Solid Earth 626 Sciences. Springer 8, pp. 129-147, Houten, Netherlands. 627 SAVOV I. P., RYAN J. G., D'ANTONIO M. & FRYER P. 2007. Shallow slab fluid release 628 across and along the Mariana arc-basin system: Insights from geochemistry of 629 serpentinized peridotites from the Mariana fore arc. Journal of Geophysical Research 630 B09205, DOI: 10.1029/2006JB004749. 631 SAVOV I. P., RYAN J. G., D'ANTONIO M., KELLEY K. & MATTIE P. 2005. Geochemistry 632 of serpentinized peridotites from the Mariana Forearc Conical Seamount, ODP Leg 125: 633 Implications for the elemental recycling at subduction zones. Geochemistry Geophysics 634 Geosystems 6, Q04J15, DOI: 10.1029/2004GC000777. 635 SCHELLART W. P., FREEMAN J., STEGMAN D. R., MORESI L. & MAY D. 2007. Evolution 636 and diversity of subduction zones controlled by slab width. *Nature* 446, 308-311. 637 SHAW A. M., HAURI E. H., FISCHER T. P., HILTON D. R. & KELLEY K. A. 2008. 638 Hydrogen isotopes in Mariana arc melt inclusions: Implications for subduction 639 dehydration and the deep-Earth water cycle. Earth and Planetary Science Letters 275, 640 138-145.
- SHEN Y. & FORSYTH D. W. 1995. Geochemical constraints on initial and final depths of
 melting beneath mid-ocean ridges. *Journal of Geophysical Research*, 100 2211-2237.

| 643 644 | SMITH W. H. F. & WESSEL P. 1990. Gridding with continuous curvature splines in tension. <i>Geophysics</i> 55, 293-305. |
|--------------------------|---|
| 645 646 | STERN R. J. 2002. Subduction Zones. <i>Reviews of Geophysics</i> 40, 37, DOI:10.1029/2001RG000108. |
| 647 648 649 650 | STERN R. J. 2010. The anatomy and ontogeny of modern intra-oceanic arc systems. <i>In</i> Kusky T.M., Zhai MG. and Xiao W. (ed.) <i>The Evolving Continents: Understanding Processes of Continental Growth</i> . Geological Society of London, Special Publication 338, pp.7-34, London, U.K. |
| 651 652 653 | STERN R. J. & BLOOMER S. H. 1992. Subduction zone infancy: Examples from the Eocene Izu-Bonin-Mariana and Jurassic California arcs. <i>Geological Society of America Bulletin</i> 104, 1621-1636. |
| 654 655 656 657 | STERN R. J., FOUCH M. & KLEMPERER S. L. 2003. An Overview of the Izu-Bonin-Mariana Subduction Factory. <i>In</i> Eiler J. and Hirschmann M (ed.) <i>Inside the subduction factory</i> . American Geophysical Union, Geophysical Monograph 138, pp. 175-222, Whashington, D.C. |
| 658 659 660 661 | STERN R. J., KOHUT E., BLOOMER S. H., LEYBOURNE M., FOUCH M. & VERVOORT J. 2006. Subduction factory processes beneath the Guguan cross-chain, Mariana Arc: no role for sediments, are serpentinites important? <i>Contributions to Mineralogy and Petrology</i> 151, 202-221. |
| 662 663 | STERN R. J., TAMURA Y., MASUDA H. <i>et al.</i> 2013. How the Mariana Volcanic Arc ends in the south. <i>Island Arc</i> 22, 133-148. |
| 664 665 | TAYLOR B. & MARTINEZ F. 2003. Back-arc basin basalt systematics. <i>Earth and Planetary Science Letters</i> 210, 481-497. |
| 666 667 668 | TIBI R., WIENS D. A. & YUAN X. 2008. Seismic evidence for widespread serpentinized forearc mantle along the Mariana convergence margin. <i>Geophysical Research Letters</i> 35, L13303, DOI: 10.1029/2008gl034163. |
| 669 670 671 672 | VAN KEKEN P. E., KIEFER B. & PEACOCK S. M. 2002. High-resolution models of subduction zones: Implications for mineral dehydration reactions and the transport of water into the deep mantle. <i>Geochemistry Geophysics Geosystems</i> 3, 1056, DOI:10.1029/2001GC000256. |
| 673 674 675 | WADA I., RYCHERT C. A. & WANG K. 2011. Sharp thermal transition in the forearc mantle wedge as a consequence of nonlinear mantle wedge flow. <i>Geophysical Research Letters</i> 38, L13308, DOI: 10.1029/2011gl047705. |
| 676 677 678 | WADE J. A., PLANK T., STERN R. J. <i>et al.</i> 2005. The may 2003 eruption of Anatahan volcano, Mariana Islands: Geochemical evolution of a silicic island-arc volcano. <i>Journal of Volcanology and Geothermal Research</i> 146, 139-170. |

| 679 680 681 | WALLACE L. M., MC CAFFREY R., BEAVAN J. & ELLIS S. 2005. Rapid microplate rotations and backarc rifting at the transition between collision and subduction. <i>Geology</i> 33, 857-860. |
|--|---|
| 682 683 | WESSEL P. & SMITH W. H. F. 1995a. New version of the Generic Mapping Tools released. EOS Transactions American Geophysical Union 76, 329, AGU, Washington, D.C. |
| 684 685 686 687 | WESSEL P. & SMITH W. H. F. 1995b. New version of the Generic Mapping Tools released. <i>EOS Transactions American Geophysical Union</i> electromic supplement [online]. [Cited 17 July 2012]. Available from http://www.agu.org/eos_elec/951546.html, AGU, Washington, D.C. |
| 688 689 690 | WESSEL P. & SMITH W. H. F. 1998. New, improved version of Generic Mapping Tools released. <i>EOS Transactions American Geophysical Union</i> 79, 579, AGU, Washington, D.C. |
| 691 692 693 | WHEAT C. G., FRYER P., FISHER A. T. <i>et al.</i> 2008. Borehole observations of fluid flow from South Chamorro Seamount, an active serpentinite mud volcano in the Mariana forearc. <i>Earth and Planetary Science Letters</i> 267, 401-409. |
| 694 | |
| 695 | Tables |
| 696 697 698 699 700 701 702 703 704 705 706 707 708 709 | Table 1: Major (wt%) element compositions of SEMFR lavas. Mg# [= atomic (Mg²+ * 100) / (Mg²+ + Fe²+)] was calculated assuming all the iron is Fe²+ on anhydrous basis. Primitive samples with 7 wt% ≤ MgO < 8 wt% were corrected on anhydrous basis by using the equations of Klein and Langmuir (1987) for Na ₈ and Fe ₈ , and Taylor and Martinez (2003) for Ti ₈ . See text for details. Sample numbers with * have no major element data reported; minor element data will be reported elsewhere. fg: fine-grained, ol: olivine, pl: plagioclase, cpx: clinopyroxene. Table 2: Overview of mean mineral compositions in basalts from each dive in the SEMFR. n: is the total number of analyses performed in one sample, s: is the number of minerals analyzed in each sample, c: core, m: mantle, st: sieve texture, r: rim, gr: groundmass, *: minerals in 1235-R12 observed in the microcrystallized basalt, while the other 1235-R12 analyses refer to minerals in the diabasic xenolith. Numbers in italics represent reverse zoning. Bold numbers represent minerals with oscillatory zoning. NA: Not analyzed. MGR: Malaguana-Gadao Ridge, SEMFR: S.E. Mariana Forearc Rift. |
| 710 | Figure Captions |
| 711 712 713 714 715 | Fig. 1: Locality maps. A) Izu-Bonin-Mariana intraoceanic arc system. The IBM magmatic arc generally lies ~ 200 km from the trench and the Mariana Trough backarc basin spreading center generally lies ~ 300 km from the trench. The arrows represent Pacific-Mariana convergence vectors from Kato et al. (2003). Yellow box shows the area of B. B) Bathymetric map of the southernmost Mariana arc-backarc basin system. Southward, the magmatic arc (white line) |

approaches the Malaguana-Gadao spreading ridge, both of which lie unusually close (~ 110 km) to the trench. Location of the Malaguana-Gadao spreading ridge is from Martinez et al. (2000). Filled colored circles show locations of YK06-12, YK08-08 Leg 2 and YK10-12 Shinkai dives and YK08-08 Leg 2 YKDT deep-tow cameras; the small circles show the locations of dredge site D27 (Bloomer & Hawkins, 1983), Shinkai 6500 dives 158 and 159 (Fryer, 1993) and dredge sites KH98-1D1 and KH98-1D2 (Sato & Ishii, 2011); triangles show the locations of KR00-03 Leg 2 Kaiko dives in Toto caldera and Malaguana-Gadao Ridge. Note that Kaiko dive 164 is near the magma chamber (MC) identified by Becker et al. (2010). The white box shows the approximate region encompassed by SEMFR. The dashed white line shows the position of the W. Santa Rosa Bank (WSRB) Fault which separates older rocks of the Santa Rosa Bank (SRB) from the SEMFR younger rocks. The red numbers are ⁴⁰Ar – ³⁹Ar radiometric ages. Map generated with GMT (Smith & Wessel, 1990, Wessel & Smith, 1995b, Wessel & Smith, 1998, Wessel & Smith, 1995a) by using a compilation from the University of New Hampshire / Center for Coastal and Ocean Mapping / Joint Hydrographic Center (Gardner, 2006, Gardner, 2007, Gardner, 2010). C) Sidescan sonar (HMR1) image of the S. Mariana convergent margin (Fryer et al., 2003) with the location of traverses by JAMSTEC submersibles during YK06-12, YK08-08 Leg 2, YK10-12 and KR00-03 Leg 2 cruises. Dark areas have high backscatter, whitish corresponds to low backscatter. The SEMFR, the Malaguana-Gadao Ridge (MGR) and Toto caldera are dominated by high backscatter, indicating that the oceanic crust or lightly sedimented basement is exposed. White dashed line denotes SEMFR axial deeps, ridges lie between the valleys. Black arrows show the opening of SEMFR (Martinez & Stern, 2009). FNVC (Fina-Nagu Volcanic Chain) represents extinct arc volcanoes.

Fig. 2: Typical bottom profiles of SEMFR encountered during seafloor traverses. A) near the trench axis (Shinkai 6500 dive 1230) and B) near the Fina-Nagu Volcanic Chain (YKDT-87). Near the trench, SEMFR flanks are dominated by steep talus slopes of lava fragments with few exposures of tilted and faulted lava flows. Talus and outcrops are covered by thin pelagic sediment. Near the Fina-Nagu Volcanic Chain (FNVC), SEMFR relief is smoother with better-preserved pillow lava outcrops covered by thin sediment. Photographs of the typical seafloor observed near the trench (C, D) and near the FNVC (E). Black star in B) shows the beginning of YKDT deep-tow camera dredging.

Fig. 3: Photomicrographs of SEMFR lavas and fine gabbro. A) Typical microporphyritic olivine – clinopyroxene basalt (sample 1230-R2) with microlitic groundmass and microphenocrysts of plagioclase (pl) and clinopyroxene (cpx). B) Fine-grained diabase xenolith (sample 1235-12) hosted by microcrystalline basalt (finer grained part to left). The diabase contains Mg-rich olivine (Fo₈₉), Mg-rich clinopyroxene (Mg# \geq 80) and normally zoned Ca-rich plagioclase (\geq 0.1 mm). In contrast, the basaltic host is more fractionated, with Fe-rich olivine (Fo₈₅₋₈₆) and Mg-rich clinopyroxene microphenocrysts (\geq 0.1 mm). Clinopyroxene in the groundmass (< 0.1 mm) are Mg-poor and coexist with Ca-poor plagioclase microlites. Clinopyroxenes in the diabase exhibit oscillatory and reverse zoning. The boundary between the two textural realms is straight, suggesting that basalt magma picked up solidified diabase. See Supporting Information S4 for more details. C) Olivine – clinopyroxene basalt from YKDT-88 containing large olivine xenocrysts surrounded by olivine-rich groundmass. D) Photomicrograph of cryptocrystalline plagioclase basalt from Shinkai dive 1235 (sample 1235-R8) hosting an amphibole gabbro xenolith (chl: chlorite, amph: amphibole). The contact between gabbro and basalt is an irregular chilled margin, suggesting that the basalt picked up solid pieces of gabbro. A second chilled

margin is observed inside the basalt, suggesting multiple magmatic injections in the basalt. E) Photomicrograph of plagioclase (pl) xenocryst observed in the Shinkai dive 1230 (sample 1230-R17). The core of the plagioclase is well-preserved and exhibits An_{91-92} content. The mantle exhibits An_{80-89} and is mostly resorbed (sieve-texture) due to the interaction plagioclase – melt. The rim is well-preserved and is An_{83-88} . Plagioclase microlites have lower An content (An < 80 %). Larger, Mg-rich clinopyroxenes (cpx) occur near the An-rich plagioclase xenocrysts (Mg # = 86 – 88), while the clinopyroxenes microlites exhibit higher range in Mg# (74 – 88). Such Anrich plagioclases are observed in the arc crust. See Supporting Information S4 for details.

Fig. 4: Major element compositional characteristics of SEMFR, MGR, Eocene forearc basalts (FABs; Reagan et al., 2010), S. Mariana Arc lavas (SMArc: 13°10'N – 11°N) which include Toto caldera lavas. All data recalculated to 100% anhydrous. A) Potash-silica diagram (Peccerillo & Taylor, 1976), showing that SEMFR lavas are low-K basalts to medium-K basaltic andesites. The grey field represents Mariana Trough BAB lavas (Gribble et al., 1996, Hawkins et al., 1990, Kelley & Cottrell, 2009, Pearce et al., 2005) and the hatched field represents Mariana Arc lavas (Kelley & Cottrell, 2009, Kelley et al., 2010, Pearce et al., 2005, Shaw et al., 2008, Stern et al., 2006, Wade et al., 2005). The small grey triangles are Malaguana-Gadao Ridge (MGR) data from Kakegawa et al. (2008) and Pearce et al. (2005). The small black triangles are data from SMA volcanoes (Kakegawa et al., 2008, Stern et al., 2013). Larger grey triangles denote MGR and larger black triangles denote Toto samples reported in this manuscript. The field for boninites is from Reagan et al. (2010). Note that SEMFR lavas mostly plot in field of Mariana Trough BAB lavas. B) FeO*/MgO vs SiO₂ diagram for medium-Fe, medium-Fe, high-Fe discrimination (Arculus, 2003); green line discriminates between tholeiitic and calk-alkaline lavas (Miyashiro, 1974). C) Mg# vs SiO₂ and D) CaO, E) Al₂O₃, F) FeO* plotted against MgO for SEMFR, MGR, and Toto caldera. When plagioclase starts crystallizing, it produces a hinge in the liquid line of descent (LLD) of Al_2O_3 . The hinge in Al_2O_3 is observed at MgO = 6 wt%; and the kink in CaO and FeO* is observed at MgO ~ 7 wt%. Therefore, primitive layar are identified with MgO \geq 7 wt%, following the method of Kelley et al. (2010). Arrows represent fractionation trends. Ol: olivine, pl: plagioclase, cpx: clinopyroxene. We used the same method as for SEMFR lavas $(MgO \ge 7 \text{ wt}\%)$ to filter the Mariana arc and Mariana Trough lavas.

Fig. 5: Variation of A) olivine Fo and B) clinopyroxene Mg# composition with whole rock Mg#. C) Variation of An content of plagioclase core with whole rock CaO (wt%) content. Olivine, clinopyroxene and plagioclase are mostly in equilibrium with their host rock. Fractional crystallization (grey arrow) removes Mg-rich minerals from the residual melt which precipitates increasingly Fe-rich minerals. The olivine-liquid equilibrium line is calculated from experimental data of Roeder and Emslie (1970) with K_D olivine − melt = 0.3 and Fe³⁺/Fe_T = 0.17 (Kelley & Cottrell, 2009). D) Olivine − Spinel Mantle Array (OSMA) diagram of Arai (1994). Cr# of spinel inclusions and Fo content of host olivine xenocrysts in Shinkai dive 1096 upper series (blue star) and in YKDT-88 lavas (pink stars) plot within OSMA. Cr# are means for each spinel inclusion and reported with the Fo content of their olivine host. Their Cr# ≥ 50 is similar to that of the southern Mariana forearc peridotite (Ohara & Ishii, 1998); whereas BAB peridotites have Cr# < 30 (Ohara et al., 2002). SEMFR peridotites (Michibayashi et al., 2009, Sato & Ishii, 2011) have Cr# and Fo contents intermediate between southern Mariana forearc peridotites and Mariana Trough BAB peridotites (Ohara et al., 2002). E) Large xenocryst of anhedral olivine (ol) with Fo₉₀₋₉₂ hosting chromium spinel (sp) and melt inclusions (MI) from sample YKDT88-R2.

Fig. 6: The ⁴⁰Ar/³⁹Ar age spectra with ³⁶Ar/⁴⁰Ar vs ³⁹Ar/⁴⁰Ar plot for samples from the SEMFR. Percentage of ³⁹Ar released during analysis is also reported.

Fig. 7: Diagrams showing variations in A) Na₈, B) Ti₈, D) K₂O/TiO₂ versus Fe₈ and C) K₂O/TiO₂ versus Ti₈. Na₈ and Ti₈ are proxies for the fraction of mantle that is melted, Fe₈ is a proxy for the depth of mantle melting (Klein & Langmuir, 1987, Pearce et al., 2005), and K₂O/TiO₂ is a proxy for the subduction input. The grey field represents Mariana Trough BAB lavas (Gribble et al., 1996, Hawkins et al., 1990, Kelley & Cottrell, 2009, Pearce et al., 2005) and the hatched field represents Mariana arc lavas (Kelley & Cottrell, 2009, Kelley et al., 2010, Pearce et al., 2005, Shaw et al., 2008, Stern et al., 2006, Wade et al., 2005). Primitive lavas from the Mariana Trough and the Mariana arc were filtered as SEMFR lavas (MgO > 7 wt%) for consistency. The FABs field is from Reagan et al. (2010). The negative correlation of Na₈ with Fe₈ of N-MORBs (grey arrow; Arevalo Jr. & McDonough, 2010) shows that more magma is produced when melting begins deeper; while in subduction-related lavas, more melting is produced shallower. SEMFR lavas have Na₈ and Ti₈ contents slightly varying with Fe₈ content, indicating homogeneous degree of mantle melting.

 Fig. 8: A) Composition ranges for coexisting olivine Fo – plagioclase An in intraoceanic arc lavas (blue field) and BABB (red outline) after Stern et al. (2006). Arc basalts have more calcic plagioclase in equilibrium with more Fe-rich olivine compared to MORB (short dashed outline), OIB (long dashed outline), and BABB. The plagioclase-olivine relationships of SEMFR lavas generally plot in the overlap between the BABB and the arc composition fields. The black triangle denotes a Toto caldera sample. B) P-T conditions of mantle-melt equilibration estimated by using the procedure of Lee et al. (2009) for SEMFR primitive lavas with MgO \geq 7 wt%. Also shown are Mariana Trough basaltic glasses (Gribble et al., 1996, Kelley & Cottrell, 2009), and the Mariana arc melt inclusions with analyzed water contents (Kelley et al., 2010, Shaw et al., 2008). The solidus is from Katz *et al.* (2003). We used Fe³⁺/Fet = 0.17 for SEMFR and Mariana Trough BABBs, Fe³⁺/Fet = 0.25 for Mariana arc lavas (Kelley & Cottrell, 2009) and Fo₉₀ for the equilibrium mantle. We used the same method as for SEMFR lavas (MgO \geq 7 wt%) to filter the Mariana arc and Mariana Trough glass for consistency. The pink field represents the slab depth beneath SEMFR (\leq 30 km – 100 km depth; Becker et al., 2005).

Fig. 9: Geodynamic evolution of SEMFR. A) The Mariana Trough is opening ~ 5 Ma ago. B) Spreading of the Mariana Trough rifts the arc lithosphere (in orange) and forms SEMFR by stretching the forearc crust (in yellow) $\sim 2.7-3.7$ Ma ago. We speculate that SEMFR is a spreading center with intense magmatic activity. C) Post-magmatic deformation of SEMFR occurred < 2.7 Ma ago, and intensely deformed the Eocene forearc crust. D) Today, SEMFR is no longer magmatically active and amagmatic extension dominates the rift. Eocene forearc is eroded with opening of the S. Mariana Trough; and actual position of the forearc is based on R/V Yokosuka YK08-08 Leg 2 and YK10-12 cruise reports (Ohara *et al.*, 2010, Ohara *et al.*, 2008). The red box highlights the area of Fig. 10.

Fig. 10: 3D model of geodynamic evolution of the SEMFR drawn after the SE Mariana lithospheric section of Gvirtzman & Stern (2004) and the tomographic images of Miller *et al.* (2006a). The cross section is drawn from the area highlighted by a red box in Fig. 9. BAB lithos.: backarc basin lithosphere. A) Opening of the S. MarianaTrough, the Malaguana-Gadao Ridge (MGR), streetches the pre-existing Eocene forearc lithosphere ~ 5 Ma ago. B) Rupturing of the

- forearc allow mantle melting, creating new SEMFR oceanic crust $\sim 2.7 3.7$ Ma ago. The red
- line shows the location of the cross section of SEMFR shown in C. C) Continuous dehydration
- of the shallow downgoing slab controlled SEMFR magmatic activity, and SEMFR had ridge
- morphology $\sim 2.7 3.7$ Ma ago. D) Today, post-magmatic rifting dominates SEMFR.

861

862

Supporting Information:

- 863 Supporting Information S1: Description of the dives
- Fig. S1.1: Cross-sections of SEMFR rifts 1, 2 and 3 from the trench
- Fig. S1.2: Dive tracks of Shinkai dives 1096, 1230 and 1235 and deep tow camera 82
- 866 Fig. S1.3: Dive tracks of YKDT 85, 86, 87 and 88.
- Fig. S1.4: Dive tracks of Shinkai dive 973 from YK06-12 cruise report and Kaiko dive 163 from
- KR00-03 Leg 2 cruise report
- Fig. S1.5: Interpreted bathymetric profile of the eastern flank of rift 1 traversed during Shinkai
- 870 dive 1096
- Fig. S1.6: Interpreted bathymetric profile of the eastern flank of rift 2 traversed during Shinkai
- 872 dive 1230
- Fig. S1.7: Interpreted bathymetric profile of the eastern flank of rift 3 traversed during Shinkai
- 874 dive 1235.
- Fig. S1.8: Interpreted bathymetric profile of the eastern flank of rift 1 traversed during Shinkai
- 876 dive 973
- Fig. S1.9: Interpreted bathymetric profile of the summit of ridge on the eastern side of rift 3
- 878 traversed during YKDT-85
- Fig. S1.10: Interpreted bathymetric profile of the eastern flank of ridge of rift 3 (central part of
- 880 SEMFR) traversed during YKDT-86
- Fig. S1.11: Interpreted bathymetric profile of YKDT-82, performed on the summit of a ridge
- between rifts 2 and 3
- Fig. S1.12: Interpreted bathymetric profile of the axial valley of rift 3 traversed during YKDT-87
- Fig. S1.13: Interpreted bathymetric profile of the eastern flank of ridge of rift 2 performed during
- 885 YKDT-88
- Fig. S1.14: Interpreted bathymetric profile of Toto caldera performed during Kaiko dive 163
- Fig. S1.15: Interpreted bathymetric profile along the Malaguana-Gadao Ridge performed during
- 888 Kaiko dive 164, near the 13°N magmatic chamber
- Table S1.1: Longitude and latitude of the dives in the SEMFR, MGR and Toto caldera with their
- depth and trench distance
- Table S1.2: Variation of the width and depth (km) of the three SEMFR rifts along axis.

892

- 893 Supporting Information S2: Sample selection and analytical techniques
- Fig. S2.1: Location of the analyzed samples, for major elements during this study, on the
- bathymetric profiles of the Shinkai dives 1096, 1230 and 1235

896

897 Supporting Information S3: Method for describing the samples

- 899 Supporting Information S4: Petrographic description and mineralogy of the samples
- 900 Fig. S4.1: SEMFR mineral compositions in clinopyroxene, plagioclase and olivine

| 901 | Table S4.1: Representative mean clinopyroxene composition |
|-----|---|
| 902 | Table S4.2: Representative mean plagioclase composition |
| 903 | Table S4.3: Representative mean olivine composition |
| 904 | Table S4.4: Representative mean spinel composition |
| 905 | |
| 906 | Supporting Information S5: Correlation between mineral abundances and whole rock chemistry |
| 907 | Fig. S5.1: Plot showing the correlation between mineral abundances and whole rock composition. |
| 908 | A) The olivine proportions are positively correlated to the whole-rock Mg# |
| 909 | |
| 910 | Supporting Information S6: Effects of the variations of the Fo content on the P-T conditions of |
| 911 | SEMFR mantle melting |
| 912 | |